

Cite this: *Catal. Sci. Technol.*, 2019,
9, 425

In situ growth of triazine–heptazine based carbon nitride film for efficient (photo)electrochemical performance†

Qiaohui Jia, Sufen Zhang, Ziwei Gao,  Peng Yang * and Quan Gu *

The inherent properties of carbon nitride and the preparation of its (photo)electrode are essential for the efficient conversion of solar energy or electricity into chemical energy in solar hydrogen production. We report the successful *in situ* growth of a compact carbon nitride polymer (CNP) 2D film with a triazine–heptazine network fragment on FTO (CNP/FTO) through an evaporation polymerization method at a relatively low temperature (450 °C) using melamine and cyanuric chloride as precursors. The CNP film makes intimate contact with the FTO substrate *via* covalent linkage of s-triazine units and FTO, which ensures more efficient interfacial charge transport. The triazine–heptazine network of CNPs allows stronger visible-light harvesting and more effective charge separation and transfer. As such, the prepared CNP/FTO photoelectrode exhibits excellent PEC performance. Its photocurrent density is around 230 $\mu\text{A cm}^{-2}$ at 1.23 V vs. RHE, which is 7.5, 176.9 and 67.6 times that of CN-Me/FTO, CN-CC/FTO, and g-C₃N₄/FTO, respectively, under simulated solar irradiation (1 sun, AM 1.5) without sacrificial reagents and cocatalysts (CN-Me/FTO and CN-CC/FTO were prepared using melamine and cyanuric chloride alone as precursor, respectively, and g-C₃N₄/FTO was fabricated by gluing bulk g-C₃N₄ powders onto a FTO substrate). Compared with previously reported metal-free carbon nitride photoanodes, our CNP film shows the best PEC performance and lower preparation temperature. Further, the prepared CNP/FTO film can be used as an economic and potential metal-free material for the electrocatalytic hydrogen evolution reaction (HER). The CNP/FTO electrode shows higher activity in the HER with low overpotential and acceptable current densities as compared to g-C₃N₄/FTO, CN-CC/FTO, and CN-Me/FTO electrodes, which is attributed to the strong contact of compact CNP film with FTO and the increased number of terminal amino groups of CNPs.

Received 10th October 2018,
Accepted 4th December 2018

DOI: 10.1039/c8cy02105h

rsc.li/catalysis

Introduction

Hydrogen has been considered to be an ideal and renewable clean energy source due to its high energy capacity and environmental friendliness. Photocatalysis, electrocatalysis, and photoelectrochemical (PEC) method are the three primary approaches for hydrogen production *via* water splitting by sunlight or electricity or both, which have been attracting a lot of attention throughout the world. Among them, PEC and electrocatalytic approaches for the conversion of solar light and/or electricity into chemical energy can achieve pure water splitting for efficient hydrogen production without sacrificial reagents as compared to photocatalytic technology for H₂ production from water (it has low efficiency; sacrificial agents are usually required, which results in the formation of by-pro-

ducts). For PEC water splitting, the most commonly used photoanode materials are metal-based inorganic semiconductors such as TiO₂, ZnO, WO₃, BiVO₄, hematite, LaTiO₂N, and so on.^{1–8} For the electrocatalytic hydrogen evolution reaction (HER) (a half-reaction of water splitting), noble metals (especially Pt-based materials) and non-noble metal-based materials^{9–20} have been used as electrocatalysts. Despite great progress in finding new materials for PEC and electrocatalytic water splitting, these reported materials contain a metal center. Therefore, it is of great importance to develop efficient metal-free materials for both PEC and electrocatalytic water splitting. Graphitic carbon nitride (g-C₃N₄) is a promising metal-free photocatalyst with a great deal of advantages, including being non-toxic, cheaper, and stable, with visible light absorption efficiency and tailorable band energy levels, which has emerged as an alternative material for PEC water splitting.^{21–25} Moreover, this metal-free g-C₃N₄ material with a tailorable polymeric structure and large number of amino groups for water adsorption and activation has been investigated as a catalyst for electrocatalytic HER.²⁶ Therefore, the carbon nitride film on FTO substrate can be used as a

Key Laboratory of Applied Surface and Colloid Chemistry, Ministry of Education, School of Chemistry and Chemical Engineering, Shaanxi Normal University, Xi'an, 710062, China. E-mail: guquan@snnu.edu.cn

† Electronic supplementary information (ESI) available. See DOI: 10.1039/c8cy02105h

bifunctional electrode to realize PEC and electrocatalytic water splitting (related reports remain extremely rare at present). However, $g\text{-C}_3\text{N}_4$ films in most cases only exhibit low activity for PEC or electrocatalytic water splitting.

The main factors affecting the (photo)electrochemical performance of the carbon nitride electrode are the structure of carbon nitride (including conjugated structure, energy band structure, and electronic structure) and the preparation of its (photo)electrode. Great efforts have been invested toward enhancing the performance of the carbon nitride electrode by modifying the conjugated structure with π -rich organic groups,^{27–29} doping,³⁰ modifying metal and metallic molecular species,^{31,32} coupling with inorganic semiconductors,^{33,34} and crystal face tailoring.³⁵ Among these modification techniques, introducing aromatic moieties or π -rich organic groups (such as phenyl and 2,6-diaminopyridine *etc.*) into the *s*-heptazine framework to modify the conjugated structure of $g\text{-C}_3\text{N}_4$ would be an effective strategy to improve the PEC performance.^{27,29} The *s*-triazine unit as the base for carbon nitride is also an aromatic π -rich moiety, which can be used to modify melon by connecting *s*-triazine with tri-*s*-triazine units to tailor the electronic properties, optical absorption, band energy levels, and photochemical performance of carbon nitride. Our previously reported work has indicated that a triazine–heptazine network bridged by different functional groups allowed stronger visible light harvesting, better conductivity, and more efficient charge separation and transport, and thus led to excellent PEC performance as compared to the $g\text{-C}_3\text{N}_4$ electrode.³⁶ Zhang *et al.* have also demonstrated that the integration of the *s*-triazine and *s*-heptazine units to form an internal triazine–heptazine donor–acceptor (D–A) heterostructure significantly narrowed the band gap and improved the conductivity and charge carrier behavior of carbon nitride, which led to enhanced solar-to-current conversion efficiencies.³⁷ Moreover, the increased in-plane tension of triazine–heptazine units probably inhibits further polymerization in the parallel direction and thus the obtained sample has an increased number of terminal amino groups ($-\text{NH}_2$). A large number of nitrogen atoms on $-\text{NH}_2$ enables effective water adsorption and increases the adsorbed H concentration, which will result in effective electrocatalytic HER performance.²⁶ For the preparation of (photo)electrodes, it is required that the method can easily utilize doping and monomer modification strategies, and the prepared film should be uniform and have close contact with the FTO substrate. Generally, the $g\text{-C}_3\text{N}_4$ -based electrodes are fabricated by coating $g\text{-C}_3\text{N}_4$ powders onto FTO glass, which results in the non-uniform thickness of the carbon nitride film and poor contact with the substrate. Recently, various direct growth methods for the fabrication of high quality carbon nitride films have been explored, including the sol–gel method, solvothermal method, thermal vapor condensation, liquid-mediated approach, and microcontact-printing-assisted access.^{21–24,27,29,30,35,36,38–40} However, the fabrication of $g\text{-C}_3\text{N}_4$ films requires a relatively higher temperature (above 500 °C) when using thermal vapor condensation and

microcontact-printing-assisted access and the photocurrent density of films prepared by the solvothermal method is still low.

Herein, in this work, we developed a facile evaporation polymerization method to grow a compact carbon nitride polymer (CNP) 2D film with a triazine–heptazine network fragment on FTO (CNP/FTO) utilizing the volatility and vaporization of cyanuric chloride and melamine raw materials at a relatively low temperature (450 °C). During the annealing, covalent linkage of *s*-triazine units and FTO through the coupling reaction between raw materials and the hydroxyl groups on the FTO surface and further polymerization/condensation allowed the growth of CNPs with a triazine–heptazine framework on the FTO substrate. For comparison, CN-Me/FTO and CN-CC/FTO prepared by using melamine and cyanuric chloride alone as precursor, respectively, and $g\text{-C}_3\text{N}_4$ /FTO fabricated by gluing bulk $g\text{-C}_3\text{N}_4$ powders onto a FTO substrate were used as the reference samples. The CNP film on FTO substrate can be used as a bifunctional electrode to realize PEC and electrocatalytic water splitting. The CNP/FTO as a photoelectrode shows boosted PEC performance with a photocurrent density of around 230 $\mu\text{A cm}^{-2}$ at 1.23 V *vs.* RHE, which is 7.5, 67.6, and 176.9 times that of CN-Me/FTO, $g\text{-C}_3\text{N}_4$ /FTO, and CN-CC/FTO (30.7, 3.4, and 1.3 $\mu\text{A cm}^{-2}$), respectively, under simulated solar irradiation (1 sun, AM 1.5) without sacrificial reagents and cocatalysts. Most importantly, compared with previously reported metal-free carbon nitride photoanodes, our CNP film shows the best PEC performance and lower preparation temperature. The excellent PEC performance of CNP/FTO can be attributed to the intimate interfacial contact between CNPs and FTO for effective interfacial charge transport and the triazine–heptazine network of CNP films for stronger visible-light harvesting, improved conductivity, and more effective charge separation and transfer. Further, the CNP/FTO as an electrode exhibits higher activity in the HER with low overpotential and acceptable current densities as compared to $g\text{-C}_3\text{N}_4$ /FTO, CN-CC/FTO, and CN-Me/FTO electrodes, which is attributed to the intimate contact of the compact CNP film with FTO and the increased number of terminal amino groups of CNPs.

Experimental

Preparation of $g\text{-C}_3\text{N}_4$ /FTO photoelectrode

All chemicals used in the experiments were of reagent grade and used as received without further purification. The $g\text{-C}_3\text{N}_4$ /FTO photoelectrode was fabricated by gluing bulk $g\text{-C}_3\text{N}_4$ powders onto a FTO substrate. Typically, the FTO glasses were washed in turn with acetone, ethanol, and DI water under continuous sonication, and then dried in a N_2 flow. The standard $g\text{-C}_3\text{N}_4$ powder was prepared through calcination of melamine at 550 °C. By dispersing a certain amount of $g\text{-C}_3\text{N}_4$ in water, a sample slurry was obtained which was spread onto the cleaned FTO glass substrate. Finally, the $g\text{-C}_3\text{N}_4$ /FTO photoelectrode was obtained after

drying at room temperature. Uncoated areas on the electrode were isolated with insulating tape.

Preparation of CNP/FTO photoelectrode

The CNP film on FTO (CNP/FTO) was prepared *via* an evaporation-polymerization method by using melamine and cyanuric chloride as precursors. Typically, the FTO glasses were washed in turn with acetone, ethanol and DI water under continuous sonication and dried in a N₂ flow. Melamine and cyanuric chloride powders (1 : 3 molar ratios) were mixed and ground using a mortar and pestle. The mixture was placed in a ceramic crucible and then the ceramic crucible was covered with the pretreated FTO glasses. After that, the crucible was heated up to 450 °C for 3 h at a heating rate of 5 °C min⁻¹ under an Ar flow (60 mL min⁻¹) in a tubular furnace to obtain the CNP/FTO photoelectrode. When using melamine or cyanuric chloride alone as precursor, the photoelectrodes obtained through the same protocol were denoted as CN-Me/FTO and CN-CC/FTO.

Characterization

The X-ray diffraction (XRD) patterns of all samples were collected on a Rigaku D/Max2550VB+/PC (Cu K α source) at a scan rate of 2.4° min⁻¹. Scanning electron microscopy (SEM) images were obtained using a HITACHI SU8220 microscope at an acceleration voltage of 5 kV. Atomic force microscopy (AFM) was performed on a Bruker Dimension ICON instrument and silicon cantilevers with resonance frequencies of $f_0 = 300$ kHz and spring constants of $k = 40$ N m⁻¹ were used. Attenuated total reflectance Fourier transform infrared (ATR-FTIR) spectra were derived with a Perkin Elmer Fourier transform infrared spectrometer GX with an ATR unit accumulating 64 scans with a resolution of 4 cm⁻¹. Solid-state ¹³C NMR spectra were recorded with a JEOL JNM-ECZ400S spectrometer. X-ray photoelectron spectroscopy (XPS) spectra were obtained on a VG ESCALAB 250 XPS system with a monochromatized Al K α X-ray source (15 kV, 200 W). Elemental analysis results were collected from a Vario MICRO system. UV/vis diffuse reflectance spectra (UV/vis DRS) were measured using a UV/vis spectrophotometer (UV-Lambda 950, Perkin Elmer). Photoluminescence (PL) spectra were obtained in the solid state with a Shimadzu RF5301 spectrofluorophotometer with an excitation wavelength of 360 nm. Time-resolved photoluminescence (TRPL) decay measurements were carried out on a time-correlated single photon counting (TCSPC) Edinburgh FLS 920 fluorescence spectrometer. Exponential fitting was performed for the luminescence decay curves by using the following equation:

$y = A + B_1 \exp\left(\frac{-t}{\tau_1}\right) + B_2 \exp\left(\frac{-t}{\tau_2}\right)$, where A is the baseline correction (y -offset), B_1 and B_2 are pre-exponential factors, and τ_1 and τ_2 are the decay time constants: the radiative process

(τ_1) and the non-radiative process (τ_2). The mean lifetimes

(τ_m) are calculated using the following equation: $\tau_m = \frac{\sum_{i=1}^n B_i \tau_i^2}{\sum_{i=1}^n B_i \tau_i}$.

Electrochemical measurements

Cyclic voltammetry measurements were performed on a CHI 760E electrochemical work station (Chenhua Instrument, Shanghai, China) in a standard three-electrode setup with a working electrode, an Ag/AgCl reference electrode, and a platinum plate counter electrode. The prepared electrode was used as the working electrode and immersed in phosphate buffer solution (mixing 15.2 ml of 0.1 M dibasic sodium phosphate with 24.8 ml of 0.1 M monobasic sodium phosphate, pH 7.0) or 0.1 M KOH solution (pH 13.1). The measurements were carried out at a scan rate of 25 mV s⁻¹. All measurements were referred to the reversible hydrogen electrode (RHE) by using the relationship E (vs. RHE) = E (vs. Ag/AgCl) + $E_{\text{Ag/AgCl}}(\text{reference}) + 0.0591 \text{ V} \times \text{pH}$ ($E_{\text{Ag/AgCl}}(\text{reference}) = 0.1976 \text{ V}$ vs. NHE at 25 °C). Tafel plots were extracted from the anodic scan.

Mott-Schottky plots of samples were measured on a CHI 760E electrochemical work station (Chenhua Instrument, Shanghai, China) in a standard three-electrode system with the prepared electrode as the working electrode, a Pt plate as the counter electrode, and Ag/AgCl as the reference electrode at an amplitude of 10 mV and frequencies of 500, 1000, and 1500 Hz, respectively. A 0.5 M Na₂SO₄ solution after removing oxygen was used as the electrolyte.

Electrochemical impedance spectroscopy (EIS) was performed in a standard three-electrode system with the prepared electrode as the working electrode, a Pt plate as counter electrode, and an Ag/AgCl as a reference electrode. The working electrode was immersed in a sodium sulfate electrolyte solution (0.5 M) and irradiated by solar light. EIS measurement was conducted in a frequency range of 0.03 Hz to 10 kHz for an amplitude of 5 mV.

Photoelectrochemical measurement

The photoelectrochemical tests were performed on a CHI 760E electrochemical work station (Chenhua Instrument, Shanghai, China) in a standard three-electrode system with a working electrode, a platinum wire counter electrode and an Ag/AgCl reference electrode. The prepared photoelectrode was used as the working electrode; it was immersed in a sodium sulfate electrolyte solution (0.5 M) and irradiated by simulated solar irradiation (1 sun, AM 1.5). Potentials were applied *versus* the Ag/AgCl reference electrode and can be converted *versus* the reversible hydrogen electrode (RHE) according to the Nernst equation as follows: E (vs. RHE) = E (vs. Ag/AgCl) + $E_{\text{Ag/AgCl}}(\text{reference}) + 0.0591 \text{ V} \times \text{pH}$ ($E_{\text{Ag/AgCl}}(\text{reference}) = 0.1976 \text{ V}$ vs. NHE at 25 °C).

Results and discussion

Growth of CNP films

The design strategy of the growth of 2D CNP film on FTO is schematically illustrated in Fig. 1a. The *s*-triazine units (C_3N_3) can be grafted onto the FTO surface through the coupling reaction between the vaporized cyanuric chloride (boiling point is 194 °C) and the hydroxyl groups on the FTO surface, which enables continuous grafting of more *s*-triazine units (C_3N_3) through the polymerization reactions between the grafted *s*-triazine units on FTO and the vaporized cyanuric chloride and sublimated melamine (sublimated at 300 °C). At higher temperature, precursors (melamine) in a ceramic crucible can be further condensed towards *s*-heptazine (C_6N_7) unit oligomers and are also capable of covalently grafting onto the FTO. In the meantime, the grafted *s*-triazine unit networks on FTO can also be further condensed. Finally, the resulting CNP film with a polymeric triazine–heptazine network is grown on the FTO surface (a photographic image of the CNP/FTO is shown in Fig. 1b). The scanning electron microscopy (SEM) and atomic force microscopy (AFM) images reveal that the CNPs on FTO glass are composed of close-packed nanoparticles and show a uniform and smooth surface

(Fig. 1c, d and f). The cross-sectional view (Fig. 1e) indicates that the CNP film has a ~ 200 nm thickness and intimate contacts with the FTO layer, which can be confirmed by AFM results (Fig. 1g and h). The scanning transmission electron microscopy (STEM)-based elemental mapping suggests the presence of C, N, O, and Cl elements in the film, further implying the condensation and polymerization of precursors towards the formation of carbon nitride based film on FTO (Fig. 1i–k).

For comparison, we have attempted to prepare carbon nitride electrodes (denoted as CN-Me/FTO and CN-CC/FTO) using melamine or cyanuric chloride alone as precursor through the same protocol, respectively. In both cases, the carbon nitride films can also be constructed on FTO (Fig. 1b) but have a lot of inadequacies as compared to the CNP/FTO electrode. When using melamine alone as precursor, the obtained CN-Me film on FTO has a very thin thickness because of the weaker interaction between melamine and the hydroxyl groups on the FTO surface (see SEM and AFM images of CN-Me/FTO in Fig. S1a and S2a–d[†]). For the CN-CC/FTO electrode (with white color and transparency, as shown in Fig. 1b), the CN-CC film with porous structure (composed of loosely stacked nanoparticles) is non-uniform and incompact (Fig. S1b and S2e–h[†]), which is due to the lower condensation and polymerization of cyanuric chloride (proved by XRD results in Fig. 2b).

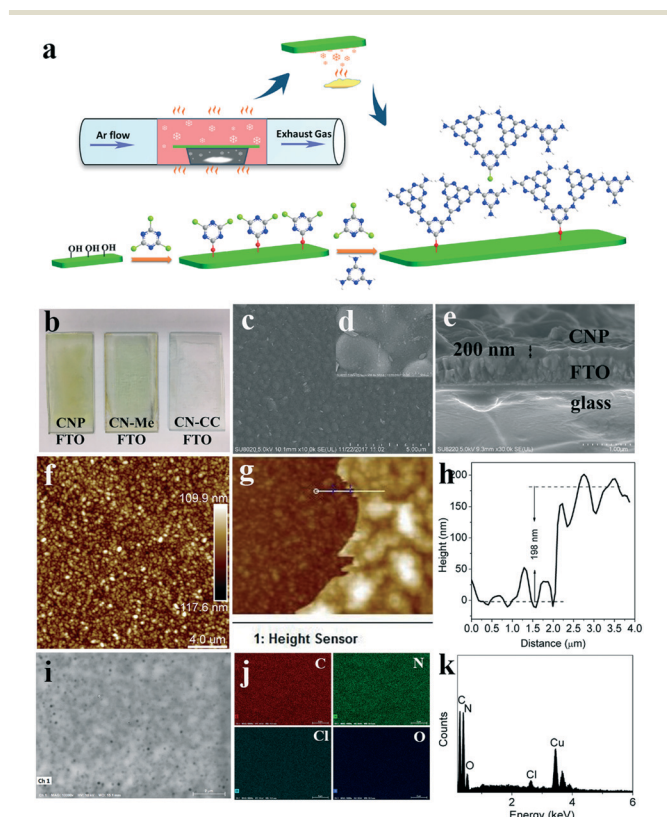


Fig. 1 (a) Schematic representation of the formation of 2D CNP film on FTO. (b) Photographic image of CNP/FTO, CN-Me/FTO, and CN-CC/FTO. (c and d) SEM images of the top view of CNP/FTO film. (e) SEM image of the cross section of CNP/FTO. (f) AFM image of surface morphology and (g and h) typical thickness of 2D CNP film. (i) STEM image, (j) corresponding elemental mapping of C, N, O, and Cl, and (k) EDS spectrum of 2D CNP film.

Structural characterizations of CNP films

To clarify the network structure of CNPs and to reveal why the CNP/FTO electrode is highly active in PEC and electrocatalytic water splitting performances, we have characterized in detail the as-prepared samples. Fig. 2a shows the XRD patterns of CN-CC/FTO, CN-Me/FTO, and CNP/FTO films. No peaks corresponding to graphitic carbon nitride can be distinguished because the film is thin and has low crystallinity (all peaks are attributed to the FTO). Then, we have tested the XRD of the CNP powder obtained by scratching the film away from the FTO substrate. As shown in Fig. 2b, the XRD pattern of the obtained CNP powder presents two diffraction peaks at 13.1° ($d \approx 0.618$ nm) and 27.3° ($d \approx 0.323$ nm) corresponding to the in-planar packing and the conjugated hexatomic heterocyclic system,^{41–50} respectively, suggesting that cyanuric chloride and melamine are polymerized towards the g - C_3N_4 analog on FTO. It is very interesting to observe that the diffraction intensity of the peak at 13.1° decreases and the diffraction peak at 27.3° shifts to the higher angle as compared to that of the bulk CN-Me powder obtained by directly heating melamine in Ar (at 27.7° , $d \approx 0.316$ nm), suggesting a decreased periodicity in the parallel direction and an increased interlayer distance between the conjugated aromatic systems of triazine–heptazine units.^{44,46,48,50} It is most likely that the incorporation of an *s*-triazine unit in melon increases the in-plane tension of the triazine–heptazine unit fragment (Fig. 1a), which is probably able to inhibit further condensation and polymerization in

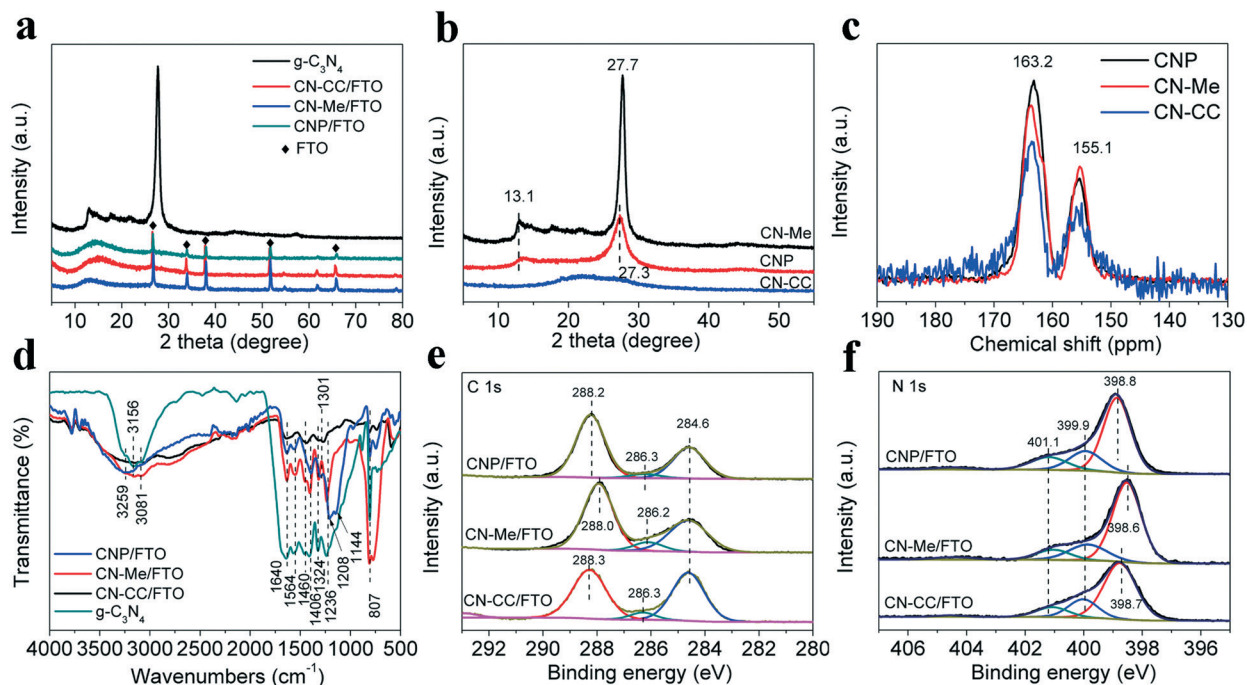


Fig. 2 (a) XRD patterns of CN-CC/FTO, CN-Me/FTO, and CNP/FTO films. (b) XRD patterns of CN-CC, CN-Me, and CNP powders obtained by scratching the film away from the FTO substrate. (c) Solid-state ^{13}C NMR spectra of CN-CC, CN-Me and CNP powders. (d) ATR-FTIR spectra of $\text{g-C}_3\text{N}_4$, CN-CC/FTO, CN-Me/FTO, and CNP/FTO films. (e and f) The high-resolution C 1s and N 1s XPS spectra of CN-CC/FTO, CN-Me/FTO and CNP/FTO films.

the parallel direction. This hypothesis can be confirmed by the solid-state ^{13}C NMR, elemental analysis, FTIR, and XPS results. As shown in Fig. 2c, the ^{13}C NMR spectrum of the CNP sample shows two distinct signals at 155.1 and 163.2 ppm corresponding to the C atoms bonded to three N atoms ($-\text{CN}_3$) and the C atoms in the $\text{N}_2\text{C-NH}_2$ unit (almost identical to the value of standard $\text{g-C}_3\text{N}_4$),^{48,51–55} which indicates the existence of characteristic *s*-heptazine units in CNPs. However, the intensity of the signal at 155.1 ppm of CNPs is lower than that of CN-Me, whereas the intensity at 163.2 ppm of CNPs is higher than that of CN-Me. This result reveals that the CNP sample has more $\text{N}_2\text{C-NH}_2$ units, which can be further confirmed by the FTIR and XPS results.

Elemental contents of the CNP powder obtained by scratching the film away from the FTO substrate were determined by elemental analysis to confirm the proposed triazine–heptazine structure and the results are summarized in Table S1.† The CN-Me and CN-CC powders obtained using melamine and cyanuric chloride alone as precursor reveal the same N/C molar ratio as that of $\text{g-C}_3\text{N}_4$ (1.53, 1.51, and 1.45 for $\text{g-C}_3\text{N}_4$, CN-Me, and CN-CC powders, respectively). The obtained CNP powder contains a small amount of residual Cl (3.5 wt%) and its N/C molar ratio is around 1.16. Such a N/C ratio is lower than the theoretical value of the N/C ratio of $\text{g-C}_3\text{N}_4$ (1.33) but higher than that of cyanuric chloride (C/N = 1.0), which implies that the CNP film on FTO has a triazine–heptazine network fragment.

Fig. 2d shows attenuated total reflectance Fourier transform infrared (ATR-FTIR) spectra of the $\text{g-C}_3\text{N}_4$, CN-CC/FTO,

CN-Me/FTO, and CNP/FTO films. The FTIR spectra of the CN-CC/FTO, CN-Me/FTO, and CNP/FTO films are largely similar to that of the bulk $\text{g-C}_3\text{N}_4$ material. They display a band at around 807 cm^{-1} corresponding to the breathing vibrations of triazine or heptazine units, a fingerprint region of $1000\text{--}1700\text{ cm}^{-1}$, and the bands in the range of $3000\text{--}3300\text{ cm}^{-1}$ for $\nu(\text{N-H})$ stretching vibrations of the secondary amines ($-\text{NH}-$) and primary amines (NH_2) or hydrogen-bonding primary amines^{42,43,56–68} (the assignments are shown in Table S2†). This result indicates the condensation and polymerization of the precursor and successful growth of carbon nitride films on FTO. In the FTIR spectra of the $\text{g-C}_3\text{N}_4$ and CN-Me/FTO, two peaks at around 1324 and 1236 cm^{-1} attributed to the stretching vibrations of the C–NH–C unit in melon^{63–67} can be clearly distinguished, indicating the *s*-heptazine based network structure of CN-Me film on FTO. Interestingly, these bands for the CNP/FTO shift to low wavenumbers (1301 and 1208 cm^{-1}) as compared to $\text{g-C}_3\text{N}_4$ and CN-Me/FTO. According to the literature,^{66,67} the absorption bands for the C–NH–C unit in melam (triazine–NH–triazine dimer) are at 1316 , 1235 , and 1206 cm^{-1} . Thus, the shifted bands can be attributed to the stretching vibrations of the C–NH–C unit in triazine–NH–heptazine, suggesting the presence of triazine–NH–heptazine fragments in the CNP film. It is noted that the increased intensity ratio of the peak at around 3259 cm^{-1} for $\nu(\text{N-H})$ stretching vibrations of $-\text{NH}_2$ to the peak at around 3081 cm^{-1} for $\nu(\text{N-H})$ stretching vibrations of $-\text{NH}-$ shows that the CNP film on FTO has more $\text{N}_2\text{C-NH}_2$ units (consistent with the ^{13}C NMR results). Moreover, compared to the

CN-Me/FTO, the CNP/FTO shows a much decreased intensity ratio of the sharp peak for the breathing vibrations of triazine or heptazine units (at 807 cm^{-1}) to the broad band for $\nu(\text{N-H})$ stretching vibrations of the $-\text{NH}-/-\text{NH}_2$ ($3000\text{--}3300\text{ cm}^{-1}$). These results indicate the lower degree of polymerization of the CNP film on FTO caused by the introduction of *s*-triazine into the *s*-heptazine based network (because the incorporation of the *s*-triazine unit increases the in-plane tension of the triazine–heptazine unit fragment and inhibits further condensation and polymerization in the parallel direction), which is consistent with the XRD result.

Then, the XPS spectra of the $\text{g-C}_3\text{N}_4$, CN-CC/FTO, CN-Me/FTO, and CNP/FTO films were tested to identify the chemical state of elements in the films (Fig. 2, S4, and S5[†]). Peak assignments of all samples are shown in Table S3[†]. For the CNP/FTO film, the C 1s signals can be fitted into three peaks centered at around 284.6, 286.3, and 288.2 eV, which can be attributed to the contaminant aromatic carbon, carbon linked to an amino function (C-NH_x , $x = 1, 2$), and sp^2 -hybridized carbon of N-C=N in the framework,^{43,69–72} respectively. The N 1s signals can be fitted into three peaks located at around 398.8, 399.9, and 401.1 eV for sp^2 -hybridized nitrogen (C-N=C) in *s*-triazine or *s*-heptazine rings, tertiary nitrogen N-(C)_3 groups, and amino function ($-\text{NH}_x$, $x = 1, 2$),^{43,69–72} respectively. Further, the calculated ratio (NH_x/N) of N atoms in $-\text{NH}_x$ to total N atoms in the sample for the CNP/FTO film increases (from 0.11 to 0.15) as compared to CN-Me/FTO and $\text{g-C}_3\text{N}_4$, which is consistent with the NMR and FTIR results. These results confirm that the CNP film with triazine–heptazine based polymeric networks was formed on FTO. It can be seen that the binding energies of C 1s peaks at 288.2 and 286.3 eV and the N 1s peak at 399.8 eV for CNP/FTO film are higher than that of CN-Me/FTO (Fig. 2e and f), which is due to the existence of Cl with a large electronegativity value. Consistently, the Cl 2p spectrum of CNP/FTO (Fig. S5b[†]) shows two Cl $2\text{p}_{3/2}$ peaks centered at 200.3 and 197.7 eV attributed to the covalent chloride C-Cl species and ionic Cl species,^{36,46,69,73,74} respectively. Clearly, the C 1s and N 1s peaks for CN-CC/FTO, CN-Me/FTO, and CNP/FTO films shift to the higher binding energy as compared to $\text{g-C}_3\text{N}_4$ powder, and peak shifts decrease in the order CN-CC/FTO > CNP/FTO > CN-Me/FTO (Fig. 2e and f and S4 and Table S3[†]). This suggests that carbon nitride films are in close contact with FTO through chemical bonding and the carbon nitride/FTO heterojunctions form at the interface between carbon nitride and FTO (Sn 3d XPS spectra of these films show peaks for FTO, and O 1s XPS spectra of these films show peaks at 530.8 and 532.1 eV for lattice oxygen and hydroxyl oxygen of FTO,⁷⁵ as shown in Fig. S5 and Table S3[†]), which enable more efficient charge transfer and enhanced (photo)electrochemical performance.

The optical and electronic properties of CNP film

The co-polymerization of *s*-triazines and *s*-heptazines evidently changes the conventional π systems, band structure,

and electronic and optical properties of carbon nitride.^{36,37,76} Thus, the band structure and charge carrier mobility of the polymers have been characterized by UV-vis DRS, transient room-temperature photoluminescence (PL) and time-resolved photoluminescence (TRPL) to reveal the efficient (photo) electrochemical performance of the CNP/FTO electrode. Fig. 3a shows the UV-vis DRS spectra of bulk $\text{g-C}_3\text{N}_4$, CN-CC/FTO, CN-Me/FTO, and CNP/FTO samples. The absorption edge of the CN-CC/FTO prepared using cyanuric chloride as precursor (421 nm, the estimated band gap is 2.96 eV) is shorter than that of bulk $\text{g-C}_3\text{N}_4$ (461 nm), which might be due to the low degree of condensation and layer packing. The CN-Me/FTO prepared using melamine as precursor exhibits the same absorption edge as bulk $\text{g-C}_3\text{N}_4$ (the estimated band gaps are 2.78 eV), suggesting that CN-Me film on FTO has the same *s*-heptazine based polymeric structure as $\text{g-C}_3\text{N}_4$. After introducing cyanuric chloride for co-polymerization, the obtained CNP/FTO presents a broadened absorption edge (up to 517 nm) and corresponding decreased band gap (around 2.58 eV) in comparison with the bulk $\text{g-C}_3\text{N}_4$ and CN-Me/FTO, which is caused by the triazine–heptazine structure.³⁷ The corresponding HOMO and LUMO positions of the samples could be determined based on the results of Tauc plots and Mott-Schottky plots (Fig. 3b–f).⁷⁷ The band structures of these samples are depicted in Fig. 3g.

The transient room-temperature photoluminescence (PL) spectra of the samples were tested at an excitation wavelength of 360 nm. As shown in Fig. 3h, the fluorescence emission peaks for $\text{g-C}_3\text{N}_4/\text{FTO}$, CN-CC/FTO, CN-Me/FTO, and CNP/FTO samples are at around 450, 430, 450, and 475 nm, respectively, which is consistent with the absorption band edge of these samples.⁷⁸ Moreover, a significantly decreased PL peak for CNP/FTO is observed, suggesting the inhibited charge recombination and the efficient charge separation of CNP/FTO.^{78–80} The improved stabilization of both electrons and holes of CNP/FTO can be further confirmed by time-resolved photoluminescence (TRPL), as shown in Fig. 3i. The luminescence decay curves of $\text{g-C}_3\text{N}_4/\text{FTO}$, CN-CC/FTO, CN-Me/FTO, and CNP/FTO samples can be fitted and described by two time constants: the radiative process (τ_1) and the non-radiative process (τ_2). Thus, the mean lifetimes (τ_m) can be calculated, which are listed in Table S4[†]. The fluorescence lifetimes of CNP/FTO are the shortest among these samples and the variation of fluorescence lifetime of samples is in good agreement with the PEC activity. This result implies that the triazine–heptazine polymeric structure of CNP film on FTO remarkably changes the charge carrier behavior and enables more effective PEC reactions.

The photoelectrochemical (PEC) properties of the CNP/FTO photoelectrode

The PEC properties of the prepared films as photoanodes (schematic illustration is shown in Fig. 4a) were measured in 0.5 M Na_2SO_4 aqueous solution (pH ≈ 7.0) under simulated solar irradiation (1 sun, AM 1.5). The optimized ratio of raw

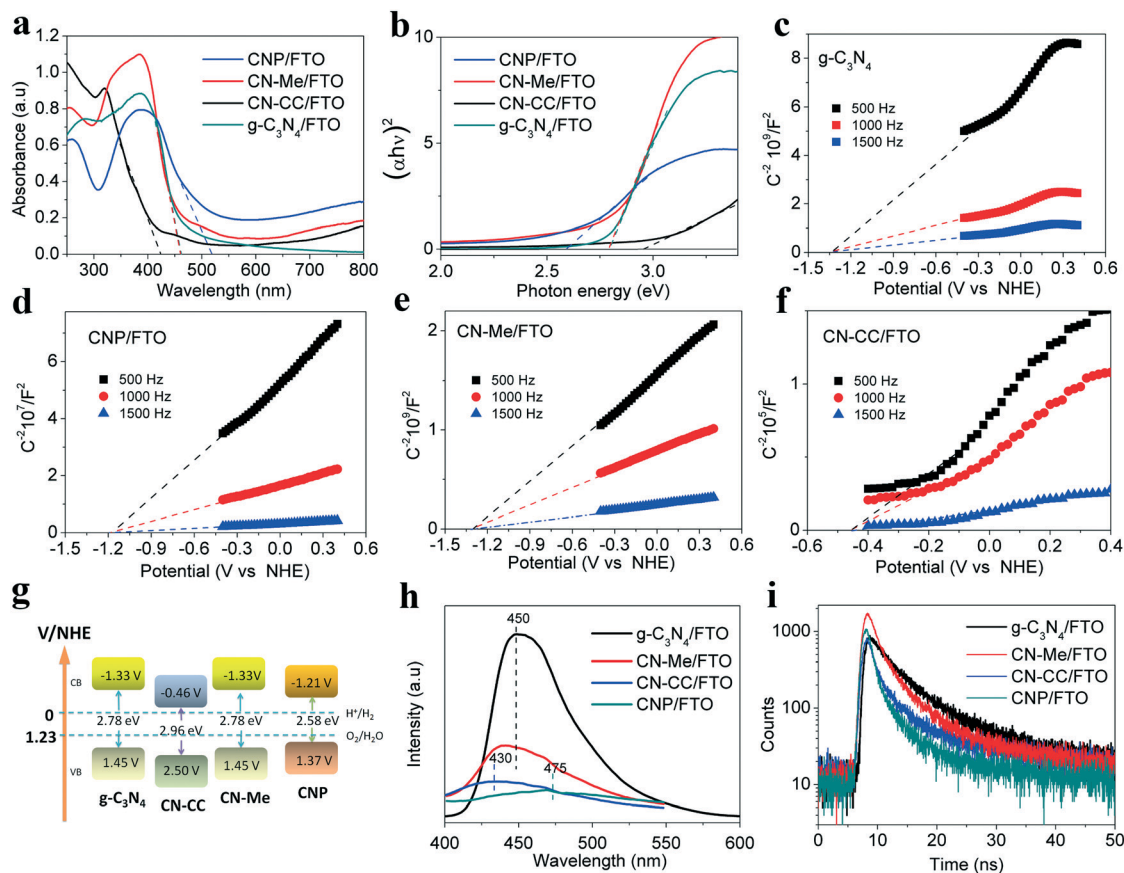


Fig. 3 (a) UV-vis DRS spectra and (b) Tauc plots of $g\text{-C}_3\text{N}_4/\text{FTO}$, $\text{CN-CC}/\text{FTO}$, $\text{CN-Me}/\text{FTO}$, and CNP/FTO samples. Mott-Schottky plots of (c) $g\text{-C}_3\text{N}_4/\text{FTO}$, (d) CNP/FTO , (e) $\text{CN-Me}/\text{FTO}$, and (f) $\text{CN-CC}/\text{FTO}$. (g) Schematic band structure of $g\text{-C}_3\text{N}_4$, CN-CC , CN-Me , and CNP films on FTO . (h) Transient room-temperature photoluminescence (PL) and (i) time-resolved photoluminescence (TRPL) spectra of $g\text{-C}_3\text{N}_4/\text{FTO}$, $\text{CN-CC}/\text{FTO}$, $\text{CN-Me}/\text{FTO}$, and CNP/FTO samples.

materials and growth time are 1:3 molar ratio of melamine and cyanuric chloride and 3 h, respectively, in terms of the PEC property, as evidenced by Fig. S6 and S7.† Fig. 4b shows the chopped linear sweep voltammetry (LSV) curves of $\text{CN-CC}/\text{FTO}$, $\text{CN-Me}/\text{FTO}$, CNP/FTO , and $g\text{-C}_3\text{N}_4/\text{FTO}$ photoanodes. The $\text{CN-CC}/\text{FTO}$ photoanode presents the lowest photocurrent density for water oxidation, which is ascribed to the weak visible-light harvesting capability and ineffective charge transfer caused by the incomplete structure with low polymerization (as evidenced by XRD and UV-vis DRS). Although CN-Me has the same polymeric structure as $g\text{-C}_3\text{N}_4$, the $\text{CN-Me}/\text{FTO}$ photoelectrode shows increased PEC performance because the close contact between the CN-Me film and the FTO surface enables more effective interfacial charge transfer. It is exciting to find that the CNP/FTO photoelectrode exhibits further increased photocurrent density with a cathodic shift in the onset potential for water oxidation in comparison with the $\text{CN-Me}/\text{FTO}$ photoelectrode. Then, we tested the chopped anodic photocurrent at an applied bias of 1.23 V vs. RHE (theoretical value of electrochemical water oxidation) of these photoelectrodes, as shown in Fig. 4c. The photocurrent density of CNP/FTO (around $230 \mu\text{A cm}^{-2}$) is 7.5, 67.6, and 176.9 times that of $\text{CN-Me}/\text{FTO}$,

$g\text{-C}_3\text{N}_4/\text{FTO}$, and $\text{CN-CC}/\text{FTO}$ (30.7 , 3.4 , $1.3 \mu\text{A cm}^{-2}$), respectively. Additionally, compared with previously reported metal-free carbon nitride photoanodes (summarized in Table S5†), our CNP film has the advantages of low preparation temperature and excellent PEC performance. These results indicate that the prepared CNP/FTO film can be used as an economic, efficient, and potential metal-free photoanode for PEC water splitting.

Based on the UV-vis DRS, PL and TRPL results (Fig. 2 and Table S4†), we can conclude that the polymeric triazine-heptazine based network structure of CNP film on FTO allows stronger visible-light harvesting and more effective charge separation and transfer. Moreover, the intimate contact between CNPs and FTO (SEM images in Fig. 1) leads to the effective interfacial charge transfer. These conclusions can be further supported by the fact that the photocurrent density of the CNP/FTO photoelectrode fabricated through the same protocol as that of the $g\text{-C}_3\text{N}_4/\text{FTO}$ photoelectrode (gluing CNP powders onto a FTO substrate) is larger than that of $g\text{-C}_3\text{N}_4/\text{FTO}$ but smaller than that of CNP/FTO (as shown in Fig. 4c). To further understand the charge-transport and interfacial charge-transfer process in the photoelectrode, we have also carried out the measurement of electrochemical

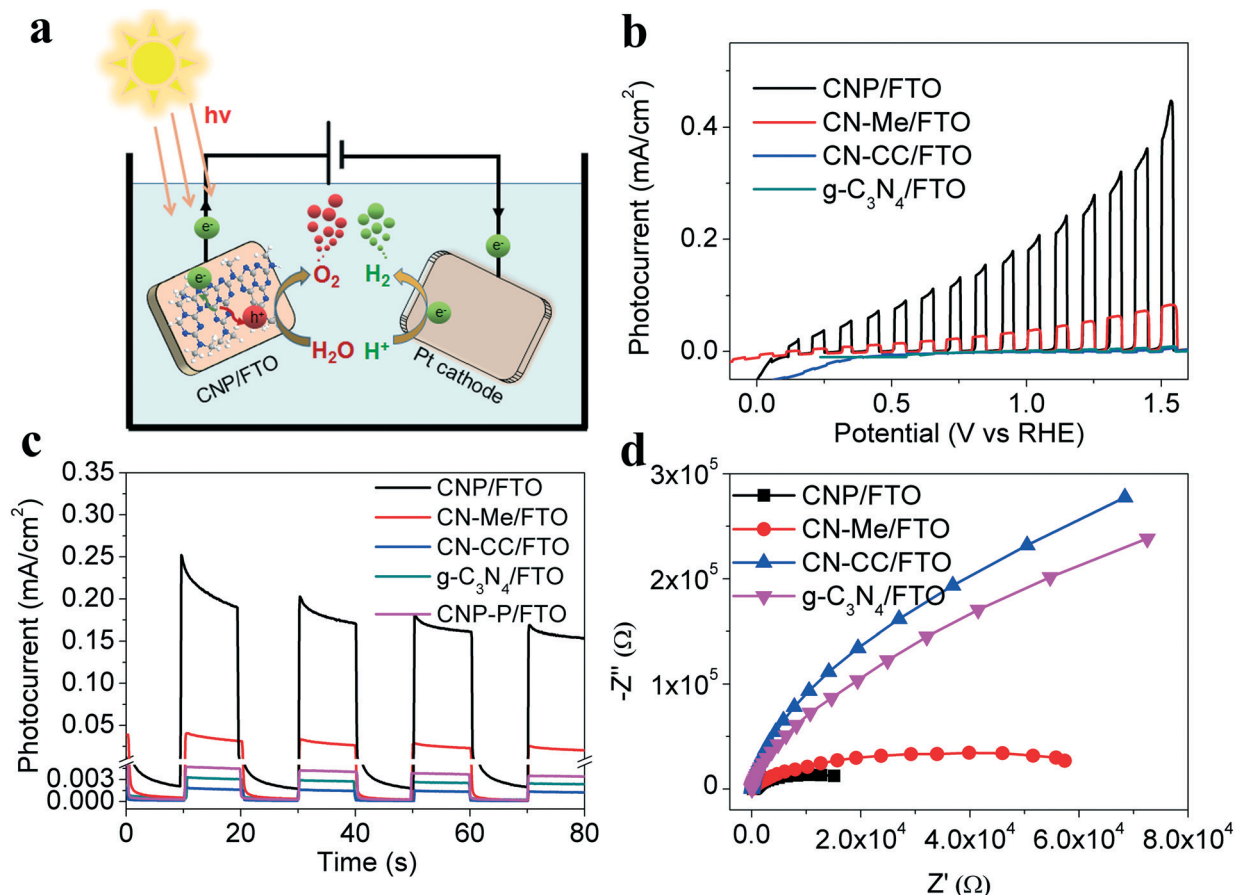


Fig. 4 (a) Schematic illustration for PEC water splitting. (b) Linear sweep voltammetry (LSV) and (c) photocurrent (i - t curve) of photoanode chopping in 0.5 M Na_2SO_4 (pH \approx 7.0) under simulated solar irradiation (1 sun, AM 1.5). (d) Electrochemical impedance spectroscopy (EIS) of photoelectrodes.

impedance spectroscopy (EIS) on these photoelectrodes under 1 sun AM 1.5 simulated solar irradiation (Fig. 4d). The CNP/FTO presents the lowest charge transfer resistance (improved conductivity) and the value of charge transfer resistance of these photoelectrodes varies in the order CNP/FTO < CN-Me/FTO < $g\text{-C}_3\text{N}_4/\text{FTO}$ < CN-CC/FTO, which is perfectly consistent with the photocurrent intensity. For the above-mentioned reasons, the CNP/FTO photoelectrode shows excellent performance for PEC water splitting.

The electrocatalytic properties for the hydrogen evolution reaction (HER) of CNP/FTO electrode

In recent years, a great deal of effort has been made to develop and find metal-free electrocatalytic materials for the HER based on low cost and abundance. Carbon nitride has appeared to be a potential metal-free material for electrocatalytic HER. Thus, we have measured the electrocatalytic HER properties of prepared electrodes in neutral and basic solution (the prepared CNP/FTO electrode is inefficient and not stable under acidic conditions, see Fig. S8[†]). Fig. 5 shows cyclic voltammetry (CV) curves of FTO, $g\text{-C}_3\text{N}_4/\text{FTO}$, CN-CC/FTO, CN-Me/FTO, and CNP/FTO measured in phosphate

buffer solution (pH 7.0) and 0.1 M KOH (pH 13.1). The CNP/FTO electrode shows higher activity in the HER with low overpotential (0.22 and 0.1 V vs. RHE for pH 7.0 and 13.1, respectively) and acceptable current densities (0.51 and 0.49 mA cm^{-2} at 0.6 and 0.3 V overpotential for pH 7.0 and 13.1, respectively) as compared to $g\text{-C}_3\text{N}_4/\text{FTO}$, CN-CC/FTO, and CN-Me/FTO electrodes. The values of overpotential and current densities of this electrode are in the same order of magnitude as those of metal-free $g\text{-C}_3\text{N}_4$ electrode and non-noble metal Ni catalyst reported in the literature.²⁶ It is found that the CV curves of FTO substrate at both pH values show a reduction peak at around 0.1 V corresponding to reduction of SnO_2 to SnO . Coating carbon nitride material on FTO prevents the direct contact between FTO and the solution, which leads to the decrease or even disappearance of this reduction peak because the charges transfer from FTO to carbon nitride for the HER. For the CNP/FTO electrode, the complete disappearance of the reduction peak indicates that the FTO substrate is completely and intimately covered with the compact CNP film. However, there is still a very small reduction peak existing on the CV curves of $g\text{-C}_3\text{N}_4/\text{FTO}$ and CN-CC/FTO electrodes, ascribed to the loosely stacked and porous structure of $g\text{-C}_3\text{N}_4$ and CN-CC films on FTO. These findings are

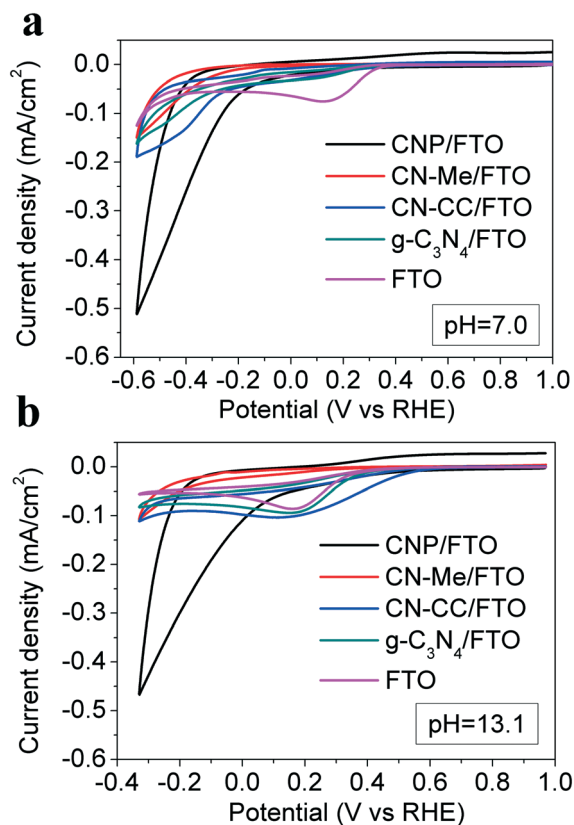


Fig. 5 Cyclic voltammetry curves of FTO, g-C₃N₄/FTO, CN-CC/FTO, CN-Me/FTO, and CNP/FTO in (a) phosphate buffer solution (pH 7.0) and (b) 0.1 M KOH solution (pH 13.1).

consistent with SEM results. Moreover, the stability of the CNP/FTO electrode was also evaluated by re-cycling the CV curve for 20 cycles using a scan rate of 25 mV s⁻¹. As shown in Fig. S9[†] after twenty scans in both electrolytes, the overpotential negligibly changed and the current density at high overpotential decreased by about 25% and 15% for pH 7 and pH 13.1, respectively.

Based on the Tafel analysis of the *J*-*V* curves (Fig. S10[†]) and ref. 26, the HER of carbon nitride follows the mechanism of adsorption and electroreduction of protons (Volmer-Heyrovsky mechanism). This means that the HER activity of carbon nitride lies on terminal amino groups carrying hydrogen. The nitrogen atoms on the terminal amino groups enable effective adsorption of water and thus lead to the increased adsorbed proton (H_a) concentration, which has a great effect on the HER (especially under alkaline conditions). The positively charged carbon atom near the electron withdrawing amino groups promotes the adsorption of OH groups. For CNP/FTO, the CNP film has an increased number of terminal amino groups (as evidenced by structural characterization such as XRD, NMR, FTIR, XPS and elemental analysis) in comparison with the CN-Me film and g-C₃N₄ because the increased in-plane tension of triazine-heptazine units inhibits further condensation and polymerization in the parallel direction. Moreover, intimate contact between the com-

compact CNP film and the FTO substrate has a great effect on efficient electron transfer and the HER. For these reasons, the CNP/FTO electrode shows enhanced electrocatalytic HER activity.

Conclusions

In summary, we have fabricated a compact CNP 2D film on FTO (CNP/FTO) by an evaporation polymerization method using melamine and cyanuric chloride as precursors. The covalent linkage of *s*-triazine units and FTO leads to the strong bonding between the CNP film and the FTO substrate, which ensures intimate contact and more efficient interfacial charge transport. Structural characterization indicates that the prepared CNP films on FTO have a triazine-heptazine network fragment, allowing stronger visible-light harvesting, more effective charge separation and transfer, and more terminal amino groups. The photocurrent density of the CNP/FTO photoanode is around 230 μA cm⁻² at 1.23 V vs. RHE, which is 7.5, 67.6, and 176.9 times that of CN-Me/FTO, g-C₃N₄/FTO, and CN-CC/FTO (30.7, 3.4, and 1.3 μA cm⁻²), respectively, under simulated solar irradiation (1 sun, AM 1.5) without sacrificial reagents and cocatalysts. Compared with previously reported metal-free carbon nitride photoanodes, our CNP film shows the best PEC performance and lower preparation temperature. The excellent PEC performance of the CNP/FTO photoelectrode could be attributed to the enhanced charge transport, effective interfacial charge transfer, and the enhanced visible light harvesting. Further, we have measured the electrocatalytic HER properties of the prepared CNP/FTO electrode in neutral and basic solution. The HER activity of the CNP/FTO electrode is higher than those of g-C₃N₄/FTO, CN-CC/FTO, and CN-Me/FTO electrodes because of the increased number of terminal amino groups in comparison with the CN-Me film and g-C₃N₄ as well as the intimate contact between the compact CNP film and FTO for efficient electron transfer.

Conflicts of interest

There are no conflicts to declare.

Acknowledgements

This work is financially supported by the National Natural Science Foundation of China (No. 21503127 and No. 21872089), the Natural Science Basic Research Plan in Shaanxi Province of China (No. 2017JM2008), and the 111 Project (B14041).

Notes and references

- 1 S. Chen, S. S. Thind and A. Chen, *Electrochem. Commun.*, 2016, **63**, 10–17.
- 2 I. S. Cho, J. Choi, K. Zhang, S. J. Kim, M. J. Jeong, L. Cai, T. Park, X. Zheng and J. H. Park, *Nano Lett.*, 2015, **15**, 5709–5715.
- 3 M. A. Norman, W. L. Perez, C. C. Kline and R. H. Coridan, *Adv. Funct. Mater.*, 2018, **28**, 1800481.

- 4 X. Li, S. Liu, K. Fan, Z. Liu, B. Song and J. Yu, *Adv. Energy Mater.*, 2018, 8, 1800101.
- 5 S. S. Kalanur, Y. J. Hwang, S. Y. Chae and O. S. Joo, *J. Mater. Chem. A*, 2013, 1, 3479–3488.
- 6 T. W. Kim and K.-S. Choi, *Science*, 2014, 343, 990–994.
- 7 Y. Zhang, H. Zhang, H. Ji, W. Ma, C. Chen and J. Zhao, *J. Am. Chem. Soc.*, 2016, 138, 2705–2711.
- 8 Y. Zhang, J. Shi, C. Cheng, S. Zong, J. Geng, X. Guan and L. Guo, *Appl. Catal., B*, 2018, 232, 268–274.
- 9 M. Gong, D.-Y. Wang, C.-C. Chen, B.-J. Hwang and H. Dai, *Nano Res.*, 2016, 9, 28–46.
- 10 W.-F. Chen, J. T. Muckerman and E. Fujita, *Chem. Commun.*, 2013, 49, 8896–8909.
- 11 S. H. Ahn, S. J. Hwang, S. J. Yoo, I. Choi, H.-J. Kim, J. H. Jang, S. W. Nam, T.-H. Lim, T. Lim, S.-K. Kim and J. J. Kim, *J. Mater. Chem.*, 2012, 22, 15153–15159.
- 12 J. R. McKone, B. F. Sadtler, C. A. Werlang, N. S. Lewis and H. B. Gray, *ACS Catal.*, 2013, 3, 166–169.
- 13 P. Zou, J. Li, Y. Zhang, C. Liang, C. Yang and H. J. Fan, *Nano Energy*, 2018, 51, 349–357.
- 14 L. Ji, C. Lv, Z. Chen, Z. Huang and C. Zhang, *Adv. Mater.*, 2018, 30, 1705653.
- 15 Y. Yin, J. Han, Y. Zhang, X. Zhang, P. Xu, Q. Yuan, L. Samad, X. Wang, Y. Wang, Z. Zhang, P. Zhang, X. Cao, B. Song and S. Jin, *J. Am. Chem. Soc.*, 2016, 138, 7965–7972.
- 16 T. Tian, L. Huang, L. Ai and J. Jiang, *J. Mater. Chem. A*, 2017, 5, 20985–20992.
- 17 J. Wan, J. Wu, X. Gao, T. Li, Z. Hu, H. Yu and L. Huang, *Adv. Funct. Mater.*, 2017, 27, 1703933.
- 18 Y.-T. Xu, X. Xiao, Z.-M. Ye, S. Zhao, R. Shen, C.-T. He, J.-P. Zhang, Y. Li and X.-M. Chen, *J. Am. Chem. Soc.*, 2017, 139, 5285–5288.
- 19 J. Xiong, W. Cai, W. Shi, X. Zhang, J. Li, Z. Yang, L. Feng and H. Cheng, *J. Mater. Chem. A*, 2017, 5, 24193–24198.
- 20 B. Ren, D. Li, Q. Jin, H. Cui and C. Wang, *J. Mater. Chem. A*, 2017, 5, 19072–19078.
- 21 J. Bian, Q. Li, C. Huang, J. Li, Y. Guo, M. Zaw and R.-Q. Zhang, *Nano Energy*, 2015, 15, 353–361.
- 22 J. Liu, H. Wang, Z. P. Chen, H. Moehwald, S. Fiechter, R. van de Krol, L. Wen, L. Jiang and M. Antonietti, *Adv. Mater.*, 2015, 27, 712–718.
- 23 X. Lv, M. Cao, W. Shi, M. Wang and Y. Shen, *Carbon*, 2017, 117, 343–350.
- 24 X. Xie, X. Fan, X. Huang, T. Wang and J. He, *RSC Adv.*, 2016, 6, 9916–9922.
- 25 J. Zhang, M. Zhang, R.-Q. Sun and X. Wang, *Angew. Chem., Int. Ed.*, 2012, 51, 10145–10149.
- 26 M. Shalom, S. Gimenez, F. Schipper, I. Herraiz-Cardona, J. Bisquert and M. Antonietti, *Angew. Chem.*, 2014, 126, 3728–3732.
- 27 J. Xu, S. Cao, T. Brenner, X. Yang, J. Yu, I. M. Antonietti and M. Shalom, *Adv. Funct. Mater.*, 2015, 25, 6265–6271.
- 28 H. Kim, S. Gim, T. H. Jeon, H. Kim and W. Choi, *ACS Appl. Mater. Interfaces*, 2017, 9, 40360–40368.
- 29 J. Bian, L. Xi, C. Huang, K. M. Lange, R.-Q. Zhang and M. Shalom, *Adv. Energy Mater.*, 2016, 6, 1600263.
- 30 Q. Ruan, W. Luo, J. Xie, Y. Wang, X. Liu, Z. Bai, C. J. Carmalt and J. Tang, *Angew. Chem., Int. Ed.*, 2017, 56, 8221–8225.
- 31 W. Zhang, J. Albero, L. Xi, K. M. Lange, H. Garcia, X. Wang and M. Shalom, *ACS Appl. Mater. Interfaces*, 2017, 9, 32667–32677.
- 32 Z. Chen, H. Wang, J. Xu and J. Liu, *Chem. – Asian J.*, 2018, 13, 1539–1543.
- 33 Y. Fang, Y. Xu, X. Li, Y. Ma and X. Wang, *Angew. Chem., Int. Ed.*, 2018, 57, 1–6.
- 34 P. Arora, A. P. Singh, B. R. Mehta and S. Basu, *Vacuum*, 2017, 146, 570–577.
- 35 X. Wei, C. Shunwei, H. Miaoyan, W. Zhenyu, L. Zhouguang and Z. Ruiqin, *ChemSusChem*, 2018, 11, 1–6.
- 36 Q. Gu, X. Gong, Q. Jia, J. Liu, Z. Gao, X. Wang, J. Long and C. Xue, *J. Mater. Chem. A*, 2017, 5, 19062–19071.
- 37 G. Zhang, L. Lin, G. Li, Y. Zhang, A. Savateev, S. Zafeiratos, X. Wang and M. Antonietti, *Angew. Chem., Int. Ed.*, 2018, 57, 9372–9376.
- 38 J. Zhang, M. Zhang, L. Lin and X. Wang, *Angew. Chem.*, 2015, 127, 6395–6399.
- 39 J. Bian, J. Li, S. Kalytchuk, Y. Wang, Q. Li, T. C. Lau, T. A. Niehaus, A. L. Rogach and R.-Q. Zhang, *ChemPhysChem*, 2015, 16, 954–959.
- 40 Y. Fang, X. Li and X. Wang, *ACS Catal.*, 2018, 8, 8774–8780.
- 41 X. Wang, K. Maeda, A. Thomas, K. Takanabe, G. Xin, J. M. Carlsson, K. Domen and M. Antonietti, *Nat. Mater.*, 2009, 8, 76–80.
- 42 P. Niu, L.-C. Yin, Y.-Q. Yang, G. Liu and H.-M. Cheng, *Adv. Mater.*, 2014, 26, 8046–8052.
- 43 H. Yu, R. Shi, Y. Zhao, T. Bian, Y. Zhao, C. Zhou, G. I. N. Waterhouse, L.-Z. Wu, C.-H. Tung and T. Zhang, *Adv. Mater.*, 2017, 29, 1605148.
- 44 Y. Kang, Y. Yang, L.-C. Yin, X. Kang, G. Liu and H.-M. Cheng, *Adv. Mater.*, 2015, 27, 4572–4577.
- 45 G. Zhang, G. Li, Z.-A. Lan, L. Lin, A. Savateev, T. Heil, S. Zafeiratos, X. Wang and M. Antonietti, *Angew. Chem.*, 2017, 129, 13630–13634.
- 46 Q. Gu, Z. Gao and C. Xue, *Small*, 2016, 12, 3543–3549.
- 47 J. Liu, Q. Jia, J. Long, X. Wang, Z. Gao and Q. Gu, *Appl. Catal., B*, 2018, 222, 35–43.
- 48 Q. Gu, Y. Liao, L. Yin, J. Long, X. Wang and C. Xue, *Appl. Catal., B*, 2015, 165, 503–510.
- 49 P. Yang, H. Ou, Y. Fang and X. Wang, *Angew. Chem., Int. Ed.*, 2017, 56, 3992–3996.
- 50 Q. Han, B. Wang, Y. Zhao, C. Hu and L. Qu, *Angew. Chem.*, 2015, 127, 11595–11599.
- 51 B. Jürgens, E. Irran, J. Senker, P. Kroll, H. Müller and W. Schnick, *J. Am. Chem. Soc.*, 2003, 125, 10288–10300.
- 52 J. R. Holst and E. G. Gillan, *J. Am. Chem. Soc.*, 2008, 130, 7373–7379.
- 53 H. Ou, L. Lin, Y. Zheng, P. Yang, Y. Fang and X. Wang, *Adv. Mater.*, 2017, 29, 1700008.
- 54 Y. Cui, Z. Ding, X. Fu and X. Wang, *Angew. Chem., Int. Ed.*, 2012, 51, 11814–11818.

- 55 J. Sun, J. Zhang, M. Zhang, M. Antonietti, X. Fu and X. Wang, *Nat. Commun.*, 2012, **3**, 1139.
- 56 M. J. Bojdys, J.-O. Müller, M. Antonietti and A. Thomas, *Chem. – Eur. J.*, 2008, **14**, 8177–8182.
- 57 H. Ou, X. Chen, L. Lin, Y. Fang and X. Wang, *Angew. Chem., Int. Ed.*, 2018, **57**, 8729–8733.
- 58 P. Yang, R. Wang, M. Zhou and X. Wang, *Angew. Chem., Int. Ed.*, 2018, **57**, 8674–8677.
- 59 X. Li, J. Zhang, L. Shen, Y. Ma, W. Lei, Q. Cui and G. Zou, *Appl. Phys. A: Mater. Sci. Process.*, 2009, **94**, 387–392.
- 60 B. V. Lotsch and W. Schnick, *Chem. Mater.*, 2006, **18**, 1891–1900.
- 61 S. Martha, A. Nashim and K. M. Parida, *J. Mater. Chem. A*, 2013, **1**, 7816–7824.
- 62 H. Liu, D. Chen, Z. Wang, H. Jing and R. Zhang, *Appl. Catal., B*, 2017, **203**, 300–313.
- 63 E. Wirnhier, M. B. Mesch, J. Senker and W. Schnick, *Chem. – Eur. J.*, 2013, **19**, 2041–2049.
- 64 T. Komatsu, *J. Mater. Chem.*, 2001, **11**, 799–801.
- 65 E. Wirnhier, M. Döblinger, D. Gunzelmann, J. Senker, B. V. Lotsch and W. Schnick, *Chem. – Eur. J.*, 2011, **17**, 3213–3221.
- 66 K. Schwinghammer, M. B. Mesch, V. Duppel, C. Ziegler, J. Senker and B. V. Lotsch, *J. Am. Chem. Soc.*, 2014, **136**, 1730–1733.
- 67 V. W.-H. Lau, M. B. Mesch, V. Duppel, V. Blum, J. Senker and B. V. Lotsch, *J. Am. Chem. Soc.*, 2015, **137**, 1064–1072.
- 68 J. Zhang, G. Zhang, X. Chen, S. Lin, L. Möhlmann, G. Dolega, G. Lipner, M. Antonietti, S. Blechert and X. Wang, *Angew. Chem., Int. Ed.*, 2012, **51**, 3183–3187.
- 69 Q. Gu, H. Sun, Z. Xie, Z. Gao and C. Xue, *Appl. Surf. Sci.*, 2017, **396**, 1808–1815.
- 70 Q. Gu, Z. Gao, H. Zhao, Z. Lou, Y. Liao and C. Xue, *RSC Adv.*, 2015, **5**, 49317–49325.
- 71 Z. Zhang, J. Huang, Y. Fang, M. Zhang, K. Liu and B. Dong, *Adv. Mater.*, 2017, **29**, 1606688.
- 72 Z. Lin and X. Wang, *Angew. Chem., Int. Ed.*, 2013, **52**, 1735–1738.
- 73 H. E. Cingil, J. A. Balmer, S. P. Armes and P. S. Bain, *Polym. Chem.*, 2010, **1**, 1323–1331.
- 74 J. Gu, M. J. Hu, Q. Q. Guo, Z. F. Ding, X. L. Sun and J. Yang, *RSC Adv.*, 2014, **4**, 50141–50144.
- 75 W. Z. Samad, M. M. Salleh, A. Shafiee and M. A. Yarmo, in *2010 IEEE International Conference on Semiconductor Electronics (ICSE2010)*, 2010, pp. 52–55.
- 76 W.-J. Ong, L.-L. Tan, Y. H. Ng, S.-T. Yong and S.-P. Chai, *Chem. Rev.*, 2016, **116**, 7159–7329.
- 77 L. Chen, M. Zhou, Z. Luo, M. Wakeel, A. M. Asiri and X. Wang, *Appl. Catal., B*, 2019, **241**, 246–255.
- 78 G. Zhang, M. Zhang, X. Ye, X. Qiu, S. Lin and X. Wang, *Adv. Mater.*, 2014, **26**, 805–809.
- 79 L. Zhang, N. Ding, J. Wu, K. Iwasaki, L. Lin, Y. Yamaguchi, Y. Shibayama, J. Shi, H. Wu, Y. Luo, K. Nakata, D. Li, X. Wang, A. Fujishima and Q. Meng, *Catal. Sci. Technol.*, 2018, **8**, 3846–3852.
- 80 Z. Luo, M. Zhou and X. Wang, *Appl. Catal., B*, 2018, **238**, 664–671.